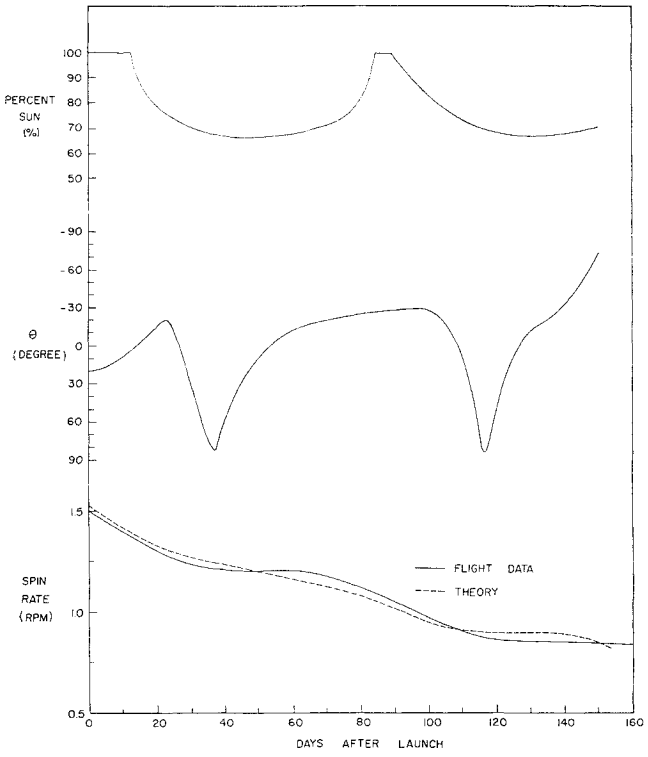

Fig. 1 Sunlight fraction $\delta(t)$ and the spin axis attitude $\theta(t)$.

empirical constant required to account for the above two assumptions. A refined analysis[2] was completed subsequently which explicitly incorporates the known histories of the spin axis attitude and percent sunlight. The net torque per satellite rotation due to each antenna boom can be expressed[2] as

$$G(t) = -\frac{pdl^2\delta(t)}{9\pi} \cdot \frac{\omega(t)T}{1+\omega(t)^2T^2}\left(2[3\alpha f_1\{\theta(t)\} + 4\beta f_2 \times \{\theta(t)\}]\, S(1) + [4\beta f_3\{\theta(t)\} - 9\alpha f_2\{\theta(t)\}]\, S'''(0)/\lambda(t)\right)$$

where t is the time into flight, p is the solar pressure on a unit area of perfectly absorbing surface normal to the incident radiation, d and l are boom diameter and length, $\delta(t)$ is the fraction of the time spent in the sunlight. The symbols α and β denote the coefficients of absorbtivity and reflectivity of the boom, $\omega(t)$ the satellite spin rate, T the boom thermal time constant, and $\lambda(t) = \rho\omega(t)^2l^4/B$, where ρ and B are the mass density (per unit length) and flexural stiffness of the boom. The spin axis attitude enters via f_1, f_2, and f_3 which are functions of the angle between the spin axis and the solar vector, $\theta(t)$.

Specifically,

$$f_1(\theta) = (1+\sin^2\theta)E(\cos\theta) - 2\sin^2\theta K(\cos\theta)$$

$$f_2(\theta) = \sin^2\theta[K(\cos\theta) - E(\cos\theta)]$$

$$f_3(\theta) = (1+\cos^2\theta)E(\cos\theta) - \sin^2\theta K(\cos\theta)$$

where K and E are complete elliptic integrals of the first and second kinds. Finally, the boom shape function $S(\xi)$, $0 \leq \xi \leq 1$, is the solution of the differential equation (a prime denotes differentiation with respect to ξ)

$$2S'''' - \lambda(1-\xi^2)S'' + 2\lambda\xi S' - 4\lambda S = 0$$

together with the appropriate boundary conditions.

Using this theory, excellent agreement was obtained[2] with the flight data for Alouette I. The purpose of this Note is to communicate similar calculations for the Explorer XX. Figure 1 contains the relevant flight data. The sunlight fraction $\delta(t)$ and the spin axis attitude $\theta(t)$ are shown. The lower part of the figure depicts the observed spin history together with the gratifying similar results of the present theory.

References

[1] Etkin, B. and Hughes, P. C., "Explanation of the Anomalous Spin Behavior of Satellites with Long, Flexible Antennae," *Journal of Spacecraft and Rockets*, Vol. 4, No. 9, Sept. 1967, pp. 1139–1145.

[2] Hughes, P. C. and Cherchas, D. B., "Influence of Solar Radiation on The Spin Behaviour of Satellites with Long Flexible Antennae," *CASI Transactions*, Canadian Aeronautics and Space Institute, Vol. 2, No. 2, Sept. 1969.

Base-Heating Measurements on Apollo Block II Command Module

WILLIAM K. LOCKMAN*
NASA Ames Research Center, Moffett Field, Calif.

Nomenclature

d	=	maximum model diameter (Fig. 1)
H_t	=	freestream total enthalpy
h_w	=	static enthalpy at model surface
l	=	model length (Fig. 1)
M_∞	=	freestream Mach number
q_b	=	base heat-transfer rate
q_{hem}	=	stagnation-point heat-transfer rate for hemispherical probe
$q_{s_{\alpha=0}}$	=	stagnation-point heat-transfer rate for model at zero angle of attack
R_b	=	base radius of model (Fig. 1)
R_c	=	corner radius of model (Fig. 1)
R_{hem}	=	radius of hemispherical probe
R_n	=	nose radius of model (Fig. 1)
$Re_{\infty,d}$	=	freestream Reynolds number based on maximum model diameter
z	=	radial coordinate in pitch plane of model (Fig. 1)
α	=	angle of attack (Fig. 1)

Introduction

NUMEROUS tunnel tests have previously been made to determine the heating to the conical afterbody of the Apollo command module (see, e.g., Refs. 1–5). However,

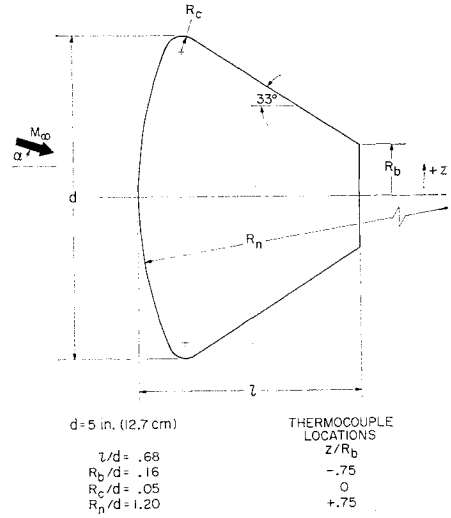

Fig. 1 Apollo Block II model.

Received September 25, 1969.
* Research Scientist. Member AIAA.

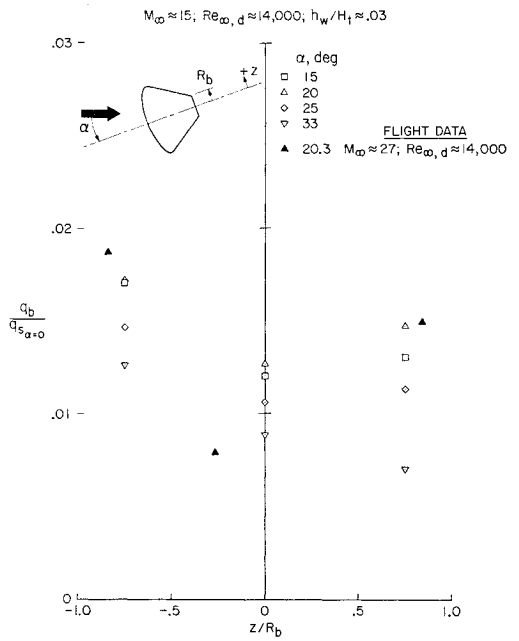

Fig. 2 Heat-transfer variation along z axis of base.

subsequent to these tests, the apex of the conical afterbody was removed to form a flat base section for docking purposes (see Fig. 1). No base-heating data were available for this new "Block II" configuration. Neither are any theories available for a satisfactory analysis of the complex three-dimensional base flow for this configuration at angle of attack. Therefore, the present shock-tunnel investigation of the heating to the base of the Apollo Block II command module was conducted to provide information necessary for a preflight assessment of the base heating and to assist in the analysis of the actual flight data. The test results are also of interest for the general study of base heating to blunt bodies at angle of attack. To eliminate any model-support interference effects on the base measurements, free-flight telemetry techniques[6-9] were used for this investigation.

Experimental Method

The tests for this investigation were performed in air in the Ames 42-in. shock tunnel at a nominal Mach number of 15, Reynolds number of 1.4×10^3 based on maximum model diameter, and total enthalpy of 4000 Btu/lbm (9.3 Mjoule/kg) with $h_w/H_t = 0.03$. Test times were approximately 20 msec. The facility, a combustion-driven shock tunnel, has a 10° half-angle conical nozzle (0.4-in. throat diameter and 42-in. exit diameter) and a 42-in.-wide hexagonal test section. The basic facility configuration, except for the nozzle and test section, and its instrumentation are the same as those described in Refs. 10–12. The tunnel calibration procedures are identical to those presented in Ref. 13.

The Apollo model tested is shown in Fig. 1. The model contained an FM telemeter circuit for each of three thermocouples located (see Fig. 1) on the thin-skin base at three radial positions of $z/R_b = -0.75$, 0, and $+0.75$ along the pitch plane through the model axis. The leeward and windward directions along the base surface are indicated by $-z$ and $+z$, respectively. Data were obtained for the flight angle-of-attack range of interest at $\alpha = 15°$, 20°, 25°, and 33°.

The telemetry system used for these tests was basically the same as that described in Refs. 6–8, with the improvements noted in Ref. 9. Each of the three telemeter units within the model consisted of a thin-skin thermocouple heating-rate sensor and a differential amplifier which controlled the frequency of an rf oscillator. The rf energy radiated directly from the oscillator tuned-circuit inductance. To isolate the telemeter units from electrical noise effects due to the hot conducting gas in the bow-shock layer and wake of the model, the model nose was made of brass and the telemeter units were completely enclosed within an electrostatic shield (see Refs. 8 and 9). The receiving system for each telemeter unit consisted of a loop antenna mounted directly on the tunnel test-section window, a vhf preamplifier, and an FM telemetry receiver with a wide-band (±1.5 MHz) frequency discriminator. The demodulated signal was recorded on a high-speed oscillograph.

For each test, the model was suspended at a given angle of attack in the tunnel test section by fine nylon threads which broke at the start of the flow, thereby releasing the model into free flight. The model inertia was sufficient to insure negligible model translation or rotation during the relatively short test time. The heating data were transmitted from the FM telemeter units in the model to the receivers and recording oscillograph located outside the tunnel. Stagnation-point heat transfer to a hemispherical probe was also monitored during the quasi-steady tunnel flow to provide a reference for the base-heating measurements.

Results and Discussion

The heat-transfer distribution along the z axis of the base, for various angles of attack, is shown in Fig. 2 and the base heat-transfer variation with angle of attack, for various base locations, is shown in Fig. 3. The data are presented with the base heating rate, q_b, normalized by the stagnation-point heating rate of the model at zero angle of attack, $q_{s_{\alpha=0}}$. The value of $q_{s_{\alpha=0}}$ was obtained for each test from the hemispherical probe heating rate, q_{hem}, with the correction for the difference in stagnation-point velocity gradient [$q_{s_{\alpha=0}} = 1.09\,(R_{hem}/R_n)^{1/2}\,q_{hem}$; see Refs. 14 and 15]. The data points are averages for several test runs. On the basis of all instrumentation errors and data scatter, the estimated maximum error in the measured $q_b/q_{s_{\alpha=0}}$ is ±15%.

For the z/R_b locations shown in Figs. 2 and 3, at a given angle of attack the heating rate decreases from the leeward to the windward side of the base with minimum heating, except for $\alpha = 33°$, near the base centerline. The higher heating rate on the leeward side could correspond to a movement of the reversed-flow stagnation point to the leeward

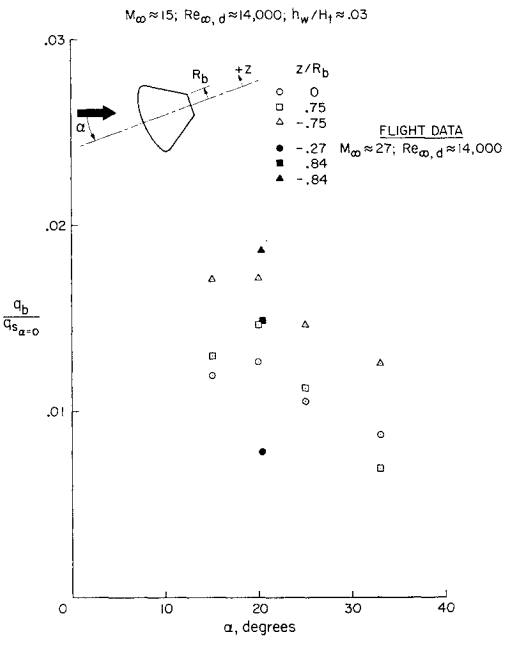

Fig. 3 Base heat-transfer variation with angle of attack.

side of the model centerline at angle of attack. The exact cause was not determined because of limitations on flow-visualization methods.

The data of Fig. 3 indicate a decrease in base heating with increasing angle of attack, except for the slight increase from $\alpha = 15°$ to $\alpha = 20°$. The increase might be explained by flow attachment occurring along the windward side of the conical afterbody for α near 20°, as reported by other investigators.[3,4] The base heating-rate levels are comparable to the levels previously measured by other investigators for the leeward separated region of the conical afterbody and show the same trend of decreased heating with increased angle of attack (see, e.g., Ref. 4).

Also shown in Figs. 2 and 3 are flight data for $\alpha = 20°$ and the same freestream Reynolds number as the tunnel tests.† For the hypersonic tunnel and flight test conditions, the base phenomena are expected to be primarily dependent on the Reynolds number and not the Mach number because of the "Mach number independence principle"[16] for blunt bodies at hypersonic speeds.[17] As with the tunnel data, the flight data indicate highest heating on the leeward side of the base and minimum heating near the base centerline. The agreement between the tunnel data and flight data is better than might be expected considering the fact that the tunnel model is a much "cleaner" configuration than the actual flight vehicle with its numerous surface cavities and protuberances. However, the results of Ref. 5 also showed no apparent difference in the heat transfer to the leeward conical afterbody with and without surface perturbations.

In conclusion, the results of this investigation have indicated highest heating on the leeward side of the base and a general decrease in base heating with increasing angle of attack. Also, the base heating-rate levels are comparable to levels previously measured for the leeward separated region of the conical afterbody. Finally, flight data for $\alpha = 20°$ and the same Reynolds number as the tunnel tests are in general agreement with the tunnel data and also indicate highest heating on the leeward side of the base.

References

[1] Jones, R. A., "Experimental Investigation of the Overall Pressure Distribution, Flow Field, and Afterbody Heat Transfer Distribution of an Apollo Reentry Configuration at a Mach Number of 8," TM X-813, 1963, NASA.

[2] Jones, J. J. and Moore, J. A., "Shock-Tunnel Heat-Transfer Investigation on the Afterbody of an Apollo-Type Configuration at Angles of Attack Up to 45°," TM X-1042, 1964, NASA.

[3] Lee, G. and Sundell, R. E., "Heat-Transfer and Pressure Distributions on Apollo Models at $M = 13.8$ in an Arc-Heated Wind Tunnel," TM X-1069, 1965, NASA.

[4] Fox, G. L. and Marvin, J. G., "An Investigation of the Apollo Afterbody Pressure and Heat Transfer at High Enthalpy," TM X-1197, 1966, NASA.

[5] Bertin, J. J., "The Effect of Protuberances, Cavities, and Angle of Attack on the Wind-Tunnel Pressure and Heat-Transfer Distribution for the Apollo Command Module," TM X-1243, 1966, NASA.

[6] McDevitt, J. B., Harrison, D. R., and Lockman, W. K., "Measurements of Pressures and Heat Transfer by FM Telemetry From Free-Flying Models in Hypersonic Tunnel Streams," *Proceedings of the First International Congress on Instrumentation in Aerospace Simulation Facilities*, INTERCON, available from P. L. Clemens, VKF/AP, Arnold Air Force Station, Tenn., Sept. 28–29, 1964, pp. 16-1to 16-12; also *IEEE Transactions on Aerospace Electronic Systems*, Vol. AES-2, Jan. 1966, pp. 2–12.

[7] Lockman, W. K., "Free-Flight Base Pressure and Heating Measurements on Sharp and Blunt Cones in a Shock Tunnel," *AIAA Journal*, Vol. 5, No. 10, Oct. 1967, pp. 1898–1900.

[8] Harrison, D. R. and Lockman, W. K., "Heat-Transfer Telemetry From Free-Flight Models in Wind Tunnels—Part 2, Using Thermocouple Sensors," AIAA Paper 68-407, San Francisco, Calif., 1968.

[9] Harrison, D. R. and Lockman, W. K., "Heat-Transfer Telemetry for Models Using Thermocouple Sensors," *Journal of Spacecraft and Rockets*, Vol. 6, No. 1, Jan. 1969, pp. 76–78.

[10] Cunningham, B. E. and Kraus, S., "A 1-Foot Hypervelocity Shock Tunnel in Which High-Enthalpy, Real-Gas Air Flows Can be Generated With Flow Times of About 180 Milliseconds," TN D-1428, 1962, NASA.

[11] Loubsky, W. J., Hiers, R. S., and Stewart, D. A.," Performance of a Combustion Driven Shock Tunnel With Applications to the Tailored Interface Operating Conditions," Third Conference on Performance of High Temperature Systems, Dec. 7–9, 1964.

[12] Marvin, J. G. and Akin, C. M., "Pressure and Convective Heat-Transfer Measurements in a Shock Tunnel Using Several Test Gases," TN D-3017, 1965, NASA.

[13] Hiers, R. S., Jr. and Reller, J. O., Jr., "Analysis of Nonequilibrium Air Streams in the Ames 1-Foot Shock Tunnel," TN D-4985, 1969, NASA.

[14] Stoney, W. E., Jr., "Aerodynamic Heating of Blunt Nose Shapes at Mach Numbers up to 14," RML 58E05a, 1958, NACA.

[15] Boison, J. C. and Curtiss, H. A., "An Experimental Investigation of Blunt Body Stagnation Point Velocity Gradient," *ARS Journal*, Vol. 29, No. 2, Feb. 1959, pp. 130–135.

[16] Hayes, W. D. and Probstein, R. F., *Hypersonic Flow Theory*, Academic Press, New York, 1959.

[17] Dewey, C. F., Jr., "Near Wake of a Blunt Body at Hypersonic Speeds," *AIAA Journal*, Vol. 3, No. 6, June 1965, pp. 1001–1010.

† These flight data are for entry of S/C 101 of Apollo-Saturn Mission 205 and were provided by D. B. Lee of NASA Manned Spaceflight Center.

ICRPG Measurement Uncertainty Model for Liquid Rockets

D. L. Colbert,* B. D. Powell,* and R. B. Abernethy†

Pratt & Whitney Aircraft, Florida Research and Development Center, West Palm Beach, Fla.

A SURVEY of the rocket industry in 1966 showed that, among the twelve companies responding to the survey, at least six different methods of treating measurement errors were in use. The Interagency Chemical Rocket Propulsion Group (ICRPG), through its Experimental Measurements Committee, sponsored the development of the ICRPG Uncertainty Model,[1] which has been accepted as a standard for the liquid rocket industry. The basis for the uncertainty model lies in the nature of measurement error, which has two components: 1) a fixed error called bias, and 2) a random error between repeated measurements which is called precision error. An index of precision error is defined

$$S = \{[\Sigma(X_i - \bar{X})^2]/(N-1)\}^{1/2} \quad (1)$$

where N is the number of measurements (X_i), and $\bar{X}$ is the average of the measurements.

An index of bias is not easily defined. Bias is the fixed, repeatable difference between the measurement and the true value of the parameter (as defined by a standard at the National Bureau of Standards). Because there is no statistic to

Presented as Paper 69-734 at the AIAA 5th Propulsion Joint Specialist Conference, U.S. Air Force Academy, Colo., June 9–13, 1969; submitted May 20, 1969; revision received October 27, 1969. We are indebted to the members of the ICRPG Experimental Measurements Committee for their participation and to Rosenblatt, Ku, and Cameron of the National Bureau of Standards for helpful discussions.

* Assistant Project Engineer.

† Program Manager.